Report on Parr Calorimetry Experiments Conducted February-March, 2019:
M. Nansteel

Summary
Six experiments were conducted using the Parr 1341 water bath calorimeter from February 27 to March 5, 2019 by BLP (Brilliant Light Power) to demonstrate excess power release from a hydrino solid fuel. The six tests included three non-control tests with active fuel and three control tests using an inert surrogate material. In each non-control test a sealed stainless steel cell containing an active fuel pellet clamped between two electrodes was immersed in the calorimeter water bath when a short burst of low-voltage high-current electrical energy from a resistance spot welder was discharged between the electrodes. The magnitude of this energy input was determined by integrating the product of the measured voltage and current during the energy input burst. The subsequent thermal energy release from the cell was determined from the temperature rise of the water bath calorimeter, properly accounting for the heat loss to the environment and stirrer input power dissipation in the water using the pre- and post-reaction water temperature change rates. In the three control tests the active fuel (~85-93 mg silver pellet) was replaced by two inert copper disks.

The raw voltage and current data from the energy input pulse and the calorimeter bath temperature data were processed and magnitudes of the energy input and thermal release were computed along with the excess energy release for each test. The excess energy is defined as the thermal energy released into the water bath in excess of the electrical energy input. For all three of the non-control tests the excess energy was positive and for two of these the excess energy was significantly greater than the cell input energy. For these two tests the energy release was about two and a half times greater than the input. In contrast, the excess energy for the three control tests was negative. In the control tests between 19 and 24% of the energy deposited in the cell was lost without being sensed by the calorimeter. It is speculated that this loss occurs by thermal conduction from the electrodes of the warm cell to the cooler arms of the resistance welder along massive copper bus bar connections. Further, this thermal loss is expected to be at least as large for the non-control tests. The large excess energy observed for the non-control tests and the fact that the measurement of thermal energy release is underestimated by the calorimeter constitute strong evidence of energy generation by the hydrino reaction in the non-control tests. Also, using the measured excess energy the average excess power was estimated for the three non-control tests. This average power ranged between about 200 and 400 kW.

Test description
All tests were conducted in a sealed one kilogram stainless steel cell. In non-control tests a single silver pellet with mass between 85 and 93 mg was clamped with a precise clamping pressure between a pair of electrodes inside the cell. Whereas in control tests the silver pellet was replaced by a pair of copper disks secured with the same clamping pressure. The cell was evacuated to 10^{-5} Torr and then filled with one atmosphere of argon gas before it was immersed in a Parr 1341 water bath calorimeter containing 1800

g of water. The electrodes which retained the silver fuel pellet or copper disks inside the cell penetrated the cell upper flange and these external electrodes were connected to the arms of a resistance spot welder[1] by massive copper bus bars. The test was initiated by a single short burst (less than the one cycle of 60 Hz power) of low-voltage high-current electrical energy from the resistance welder. The electrical energy input to the cell was measured by time integration of the voltage and current at the electrodes, and in non-control tests also by integration of the voltage and current supply to the welder. The subsequent thermal energy release from the cell to the waterbath was measured by standard calorimetric analysis of the bath temperature rise. Three non-control tests and three control tests were performed as tabulated in Table 1.

Table 1. Six tests analyzed

022719 Test 1
022719 Test 2
022819 Test 1
022819 Control Test 2
030519 Control Test 1
030519 Control Test 3

Electrical energy input

The electrical configuration of the test system is shown schematically in Fig. 1. Electrode voltage (V) was measured by a TA041 Pico voltage differential probe (700 V, 25 MHz max) and current flow (I) was monitored using an LF 30 kA Rogowski coil. Voltage and current were sampled at 100 kHz corresponding to one measurement of V and I every 10 μs. This corresponds to about 1667 V-I samples during one 60 Hz power input cycle (16.67 ms). A record of the raw voltage and current vs. time data for the duration of the electrical power input burst was obtained from BLP as a single Excel worksheet file for each test. The raw V and I data were subsequently plotted versus time and then further processed to obtain input power and energy. Voltage and current data were plotted versus time for each test in order to better characterize the input power burst and identify regions of waveform distortion, as described below.

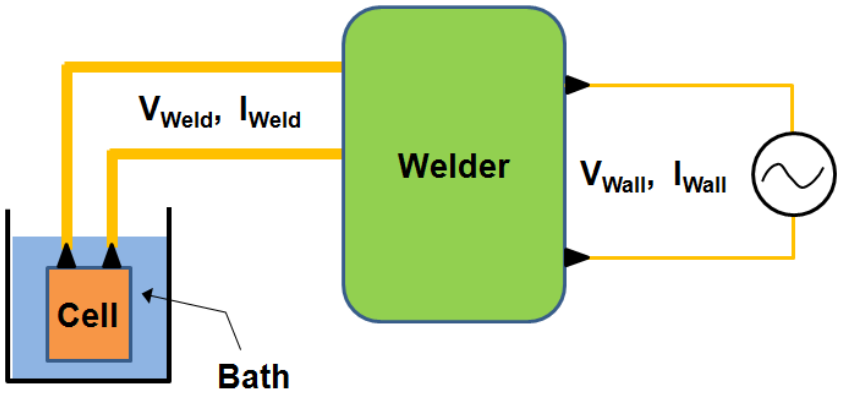

[1] LORS Machinery Model 1100AP, 1000 kVA@50% duty cycle, 60 Hz.

Figure 1. Schematic diagram of cell, calorimeter bath and welder

During the power input burst the cell electrodes are energized for approximately 10 to 13.5 ms with a variable voltage which is generally less than about 5 V. During this time the current flow is several kA and therefore hundreds of joules are deposited in the silver pellet (non-control) or copper disks (control). In the case of non-control tests, the silver pellet experiences a very rapid and violent explosion in the late stages of the process. This event has been observed directly (outside the cell) and is known to be accompanied by a strong shock wave and intense high energy ultraviolet emission. For this reason this event is referred to as detonation of the pellet. In the present tests this detonation results in an almost instantaneous spurious increase in the indicated voltage due to an electromagnetic pulse (EMP). The EMP arises directly from the detonation and precludes accurate power and energy calculations from this time forward. For this reason BLP also measured the voltage and current of the power supplied to the resistance welder, denoted here as the wall voltage and current, cf. Fig. 1. The pre-detonation welder/cell electrode voltage and current data, V_{Weld} and I_{Weld}, were supplemented by these wall data, post-detonation, in order to more accurately determine the electrical energy deposition in the cell, as described below. The wall data, V_{Wall} and I_{Wall}, were collected by the same instrumentation as the welder voltage and current, at the same sampling rate, and were included in the Excel data worksheets supplied by BLP.

The following energy calculations were conducted using the supplied V and I data for non-control tests (silver pellet):

$$E_{Weld,Predet} = \int_{t_0}^{t_{det}} \left|IV\right|_{Weld} dt$$

$$E_{Wall,Predet} = \int_{t_0}^{t_{det}} \left|IV\right|_{Wall} dt \qquad (1)$$

$$E_{Wall,Postdet} = \int_{t_{det}}^{t_f} \left|IV\right|_{Wall} dt$$

Here t is time and the product IV is the instantaneous power measured either at the welder/cell electrodes (subscript Weld) or at the welder/wall power connections (subscript Wall). The integrals in (1) were approximated by trapezoids, each with a panel width of 10 μs, the time elapsed between consecutive measurements of voltage and current. The time t_0 is the time that the welder voltage pulse is initiated, t_{det} is the time of fuel pellet detonation determined from the initial distortion of the V_{Weld} waveform for non-control tests, and t_f is the time at the end of the power pulse when the product IV is zero at the electrodes.

Although voltage and current changed sign during the pulse for both the welder and wall, resulting in positive and negative values of the product IV, the energy was calculated using the absolute value of IV. This procedure yielded the largest possible magnitude for

the various input energy quantities. The total energy input to the cell in non-control tests was calculated as

$$E_{Weld,Total} = E_{Weld,Predet} + \varepsilon E_{Wall,Postdet}$$

$$\varepsilon = \frac{E_{Weld,Predet}}{E_{Wall,Predet}}, \quad \text{welder efficiency} \qquad (2)$$

This approach, suggested by BLP, avoids the use of the distorted voltage waveform V_{Weld} during and after pellet detonation: $t_{det} \le t \le t_f$. Instead, it assumes that the post-detonation energy input to the cell from the welder is some fraction ε, the welder efficiency, of the energy supplied to the welder from the wall during that time. The welder efficiency is calculated from the pre-detonation energies of the welder and wall, cf. (2). Because the welder efficiency is based on the pre-detonation waveforms but is used to determine the post-detonation welder energy, the approach used in (2) may not be very accurate. A more conservative approach would be to use the maximum energy input, corresponding to 100% welder efficiency:

$$E_{Weld,Total,Max} = E_{Weld,Predet} + E_{Wall,Postde} \qquad (3)$$

For the control tests no detonation occurs and therefore no distorted waveforms result so the total welder and wall energy, and welder efficiency are

$$E_{Weld,Total} = \int_{t_0}^{t_f} |IV|_{Weld}\, dt$$

$$E_{Wall,Total} = \int_{t_0}^{t_f} |IV|_{Wall}\, dt \qquad (4)$$

$$\varepsilon = \frac{E_{Weld,Total}}{E_{Wall,Total}}$$

The plots of voltage, current and power vs. time for each of the six tests are given in Appendix 1. The welder voltage has a peak magnitude near 5 V and welder current peak magnitudes are near 15 kA in the first half of the pulse and 30 kA in the second half. Similarly, welder power peaks near 75 kW in the first half of the pulse and around 150 kW in the second half. In the non-control tests, Figs. A1.1-A1.3, silver pellet detonation occurs in the second half of the pulse between about 8 and 10 ms after the pulse start. This typically results in a large excursion of the welder voltage from about 5 V to 35-45 V. The wall voltage is impacted far less by the detonation in the non-control tests and this is the reason for its use in Equation (2) to calculate the total energy supplied by the welder to the cell.

Calculated energy and welder efficiency data are tabulated in Table 2 along with the detonation time measured from the start of power input in the non-control tests. The pre-detonation welder and wall energy in the non-control tests vary widely. This is due in part to the varying time of detonation. In tests with early or late detonation the pre-detonation energy was smaller or larger, respectively. This had the opposite effect on the post-detonation wall energy, cf. Table 2. Further, this resulted in highly variable welder total energy in the non-control tests. In contrast, the welder total energy in the three control tests was quite consistent. The variability of the welder efficiency in the non-control tests is most likely due to the varying detonation time, however, the efficiency is also variable in the control tests. This reinforces the argument for the use of (3) rather than (2) to obtain a conservative (upper bound) estimate of the welder total input energy. Note, Table 2, that this upper bound for the welder total input exceeds the estimate obtained using the efficiency (2) by only a small fraction.

Table 2. Welder and wall energy summary

Test	t_{det} [ms]	$E_{Weld,Predet}$ [J]	$E_{Wall,Predet}$ [J]	ε [1]	$E_{Wall,Postdet}$ [J]	$E_{Weld,Total}$ [J]	$E_{Weld,Total,Max}$ [J]
022719(1)	8.81	292.16	443.80	0.6583	44.48	321.44	336.64
022719(2)	9.88	443.30	502.20	0.8827	23.28	463.85	466.58
022819(1)	7.95	192.55	345.63	0.5571	71.89	232.60	264.44
022819(C2)				0.7928		646.86	
030519(C1)				0.7777		638.39	
030519(C3)				0.6890		600.24	

Bath thermal energy absorption

The energy release from the cell was determined from the calorimeter bath temperature history using the instructions given in the Parr 1341 Operating Instruction Manual (204M). This procedure is summarized by the equation

$$E_{out} = C\left\{(T_c - T_a) - \left[\left(\frac{dT}{dt}\right)_{pre}(t_b - t_a) + \left(\frac{dT}{dt}\right)_{post}(t_c - t_b)\right]\right\} \quad (5)$$
$$= C\Delta T$$

where E_{out} is the thermal energy released to the bath due to the input electrical energy pulse and any subsequent reaction. Subscripts a and c refer to the time of the input electrical energy pulse and the time, post-event, when the bath temperature begins a mostly linear temperature decay, respectively. The subscript b refers to the time when the bath temperature reaches 60% of the total rise from T_a to T_c: $T_b = T_a + 0.60(T_c - T_a)$. The temperature-time derivatives $(dT/dt)_{pre}$ and $(dT/dt)_{post}$ appearing in (5) are the measured slopes prior to time t_a (pre-period) and after time t_c (post-period), respectively, and C is the effective heat capacity of the calorimeter-cell system which was determined by BLP in calibration experiments: C = 12,300 J/K. In the calibration experiments C was derived by dissipating a known power burst in a resistive load inside the cell.

The term ΔT is the bath temperature rise corrected for energy transfer between the bath and the laboratory due to heat transfer and stirring input power. The correction is the term appearing in square brackets in (5). Denoting this correction term by $-\delta T$ results in

$$\Delta T = (T_c - T_a) + \delta T$$

To minimize measurement uncertainty in E_{out} the correction term should be a small fraction of the corrected temperature rise ΔT. This was achieved by careful adjustment of the bath temperature prior to the pre-period, resulting in a slightly negative temperature-time gradient during the pre- and post-periods. This was accomplished by adding water of the appropriate temperature to the bath and subsequently removing the same mass of water in order to maintain a constant bath heat capacity. Bath temperature was measured by a thermistor probe with 0.001°C resolution using a 1 Hz sampling rate.

The raw bath temperature-time data and the room temperature-time variation for each test was supplied by BLP in an Excel worksheet. These data were copied to a blank worksheet which was used to determine the parameters required in Equation (5). The temperature and time at the energy input pulse, t_a, and at the start of the post-period, t_c, were identified directly from the raw bath temperature-time data and the temperature T_b was determined by calculation from T_c and T_a. The time t_b was determined by an average of the time stamps corresponding to bath temperature T_b. The slopes during the pre- and post-periods were determined by straight line fits to the data during the respective periods. The raw temperature-time data are displayed in Appendix 2 for each test along with each of the required parameters in Equation (5) and the computed value of the energy release, E_{out}. The results are tabulated in Table 3. Note that the tests generally required about 30 minutes including the pre- and post-periods, with the actual bath temperature rise taking place during a roughly 15 minute interval, cf. Appendix 2. The corrected bath temperature rise ΔT ranged from about 0.04 to 0.065°C and energy release varied from about 484 to 796 J with higher magnitudes occurring in the non-control tests. The temperature correction δT was always less than 23% of ΔT, cf. Table 3. During each test the room temperature varied by less than about a degree, cf. Appendix 2.

Table 3. Parr calorimetry results

Test	ΔT [°C]	δT [°C]	$\delta T/\Delta T$ [1]	E_{out} [J]
022719(1)	0.0647	0.0107	0.1659	796.3
022719(2)	0.0586	0.0036	0.0613	720.7
022819(1)	0.0492	0.0062	0.1263	605.4
022819(C2)	0.0401	0.0091	0.2264	492.9
030519(C1)	0.0401	0.0071	0.1766	492.9
030519(C3)	0.0393	0.0033	0.0844	483.6

Energy balances

The energy balances for the six tests are summarized in Table 4 including the excess energy $E_{out} - E_{Weld,Total}$ and the energy ratio $E_{out}/E_{Weld,Total}$. For all three of the non-control tests the excess energy is positive and for two of these the excess energy is

significantly greater than the cell energy input $E_{Weld,Total}$. For these two tests the energy release is about two and a half times greater than the input. In contrast, the excess energy for the three control tests is negative. For these three tests the results indicate that between 19 and 24% of the electrical energy deposited in the cell is lost without being sensed by the calorimeter. This loss can only occur via some path which circumvents the bath water. Perhaps this occurs by thermal conduction along the copper bus bars which connect the warm cell electrodes to the cooler arms of the resistance welder. This conjecture is highly plausible since a copper conductor with 1 cm^2 cross section and 5 cm length passes almost 100 J of energy in ten minutes when a temperature differential of only 0.2 K is maintained between the ends of the conductor. In any case this thermal loss is expected to be at least as large for the non-control tests because the bath temperature rise in these tests is greater, indicating higher cell temperature. Therefore the excess energy in the non-control tests probably exceeds the values tabulated in Table 4. The large excess energy observed for the non-control tests and the fact that the measurement of thermal energy release is underestimated by the calorimeter constitute strong evidence of energy generation by the reaction in the non-control tests.

Table 4. Energy balance summary

Test	E_{out} [J]	$E_{Weld,Total}$ [J]	$E_{out} - E_{Weld,Total}$ [J]	$E_{out}/E_{Weld,Total}$ [1]
022719(1)	796.3	321.4	474.9	2.48
022719(2)	720.7	463.9	256.8	1.55
022819(1)	605.4	232.6	372.8	2.60
022819(C2)	492.9	646.9	-154.0	0.762
030519(C1)	492.9	638.4	-145.5	0.772
030519(C3)	483.6	600.2	-116.6	0.806

It is reasonable to assume that the release of excess energy $E_{out} - E_{Weld,Total}$ in the three non-control tests begins with detonation of the silver pellet. The precise duration of the excess energy release is unknown, however, in Table 5 the average excess power is tabulated by assuming that the release begins at detonation, t_{det}, and persists until welder power input to the cell ceases at time t_f. The excess power calculated in this way ranges between about 200 and 400 kW for the three non-control tests, cf. Table 5.

Table 5. Average excess power release during the time $t_{det} \le t \le t_f$

Test	$t_f - t_{det}$ [ms]	$E_{out} - E_{Weld,Total}$ [J]	$(E_{out} - E_{Weld,Total})/(t_f - t_{det})$ [kW]
022719(1)	1.19	474.9	399
022719(2)	0.92	256.8	279
022819(1)	1.75	372.8	213

Because of the uncertainty in the value of $E_{Weld,Total}$ for the non-control tests introduced by the use of the welder efficiency in (2), energy balance data has been re-tabulated in Table 6 using the maximum input energy $E_{Weld,Total,Max}$ as a basis. The excess energy for the non-control tests is seen to be reduced only modestly by the use of this upper limit for the input energy.

Table 6. Energy balance summary based on maximum input energy

Test	E_{out} [J]	$E_{Weld,Total,Max}$ [J]	$E_{out} - E_{Weld,Total,Max}$ [J]	$E_{out}/E_{Weld,Total,Max}$ [1]
022719(1)	796.3	336.6	459.7	2.37
022719(2)	720.7	466.6	254.1	1.54
022819(1)	605.4	264.4	341.0	2.29

Appendix 1. Electrical energy input data plots

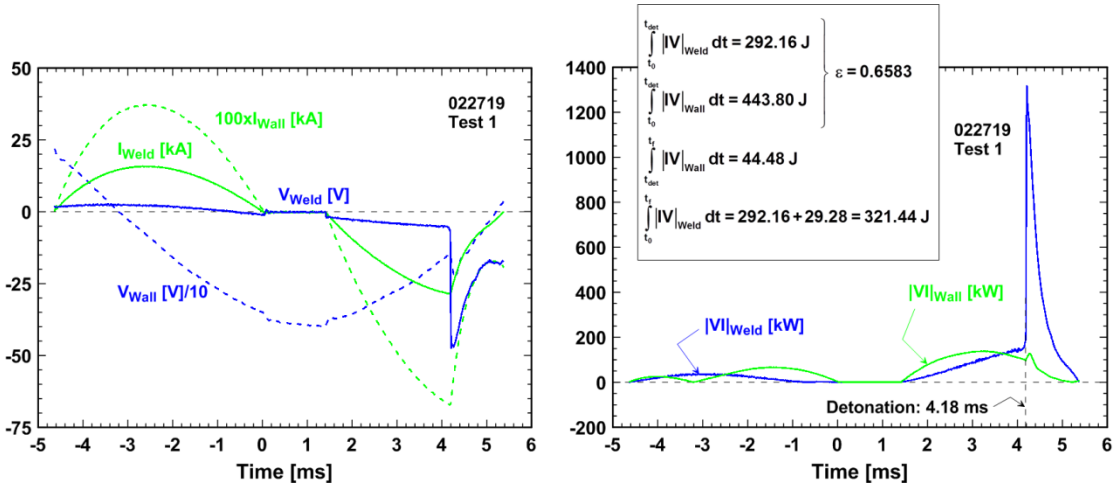

Figure A1.1. 022719 Test 1 energy input plots

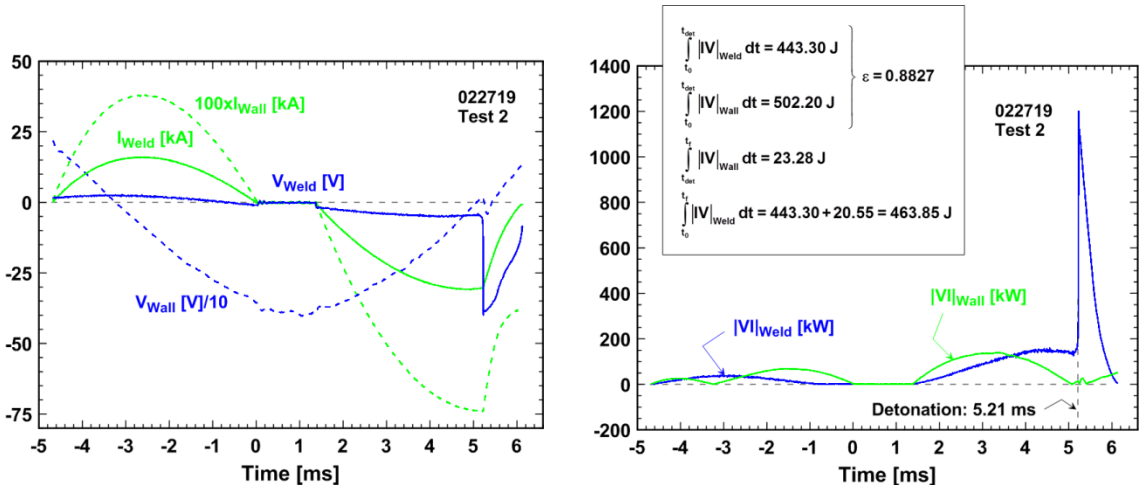

Figure A1.2. 022719 Test 2 energy input plots

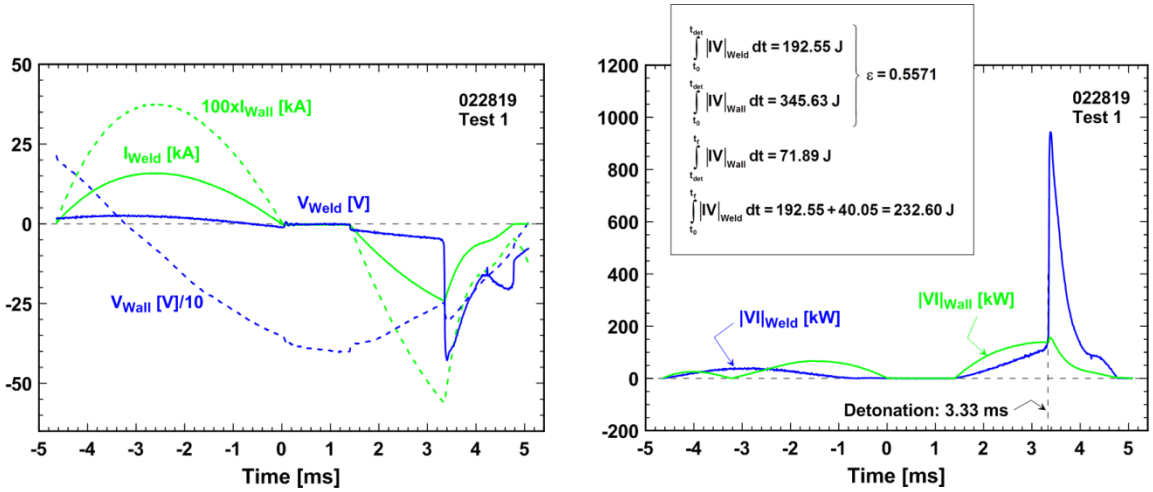

Figure A1.3. 022819 Test 1 energy input plots

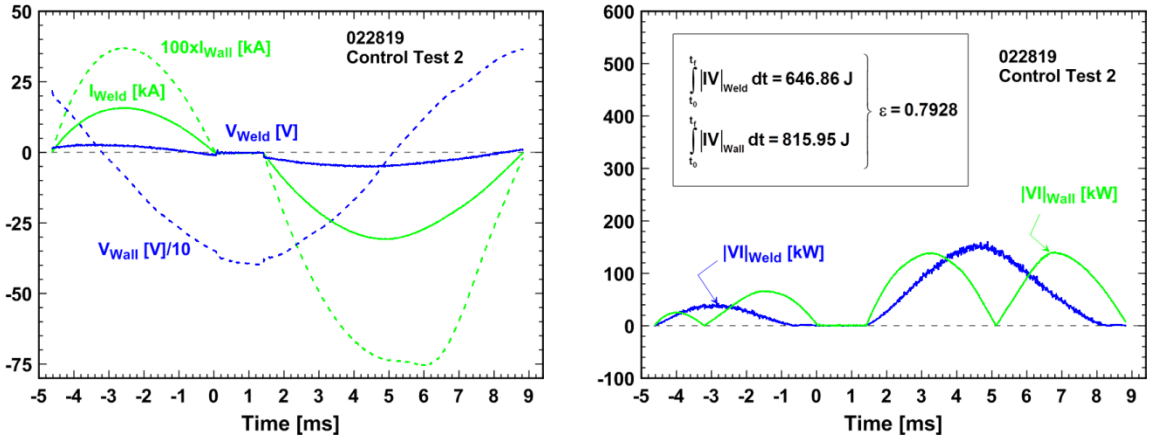

Figure A1.4. 022819 Control Test 2 energy input plots

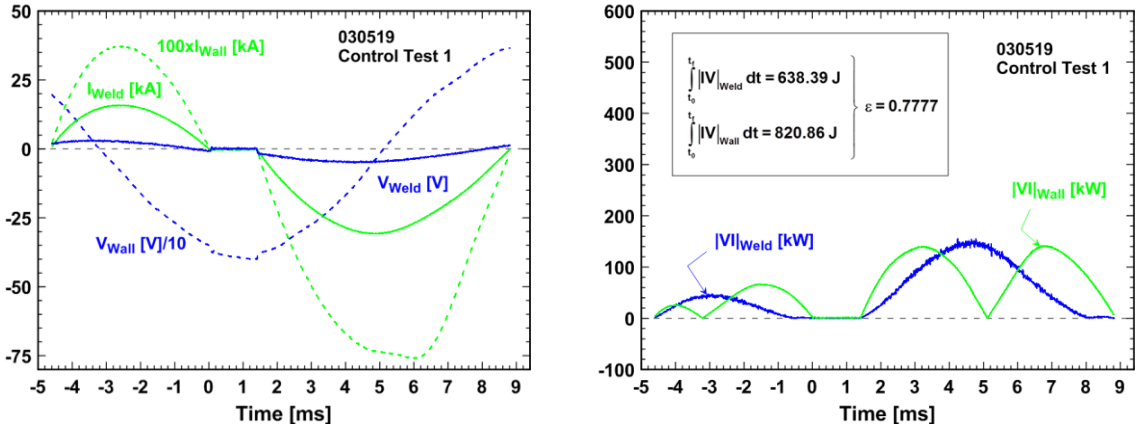

Figure A1.5. 030519 Control Test 1 energy input plots

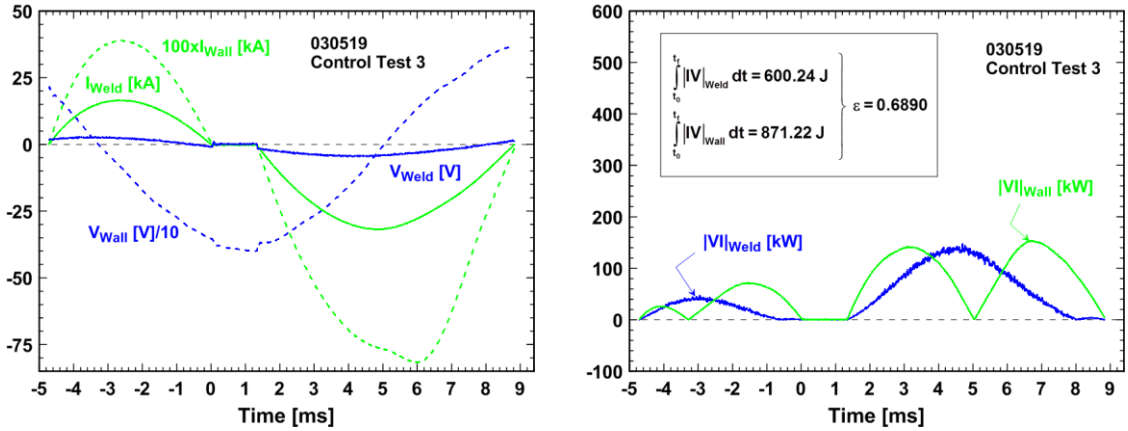

Figure A1.6. 030519 Control Test 3 energy input plots

Appendix 2. Parr calorimetry plots

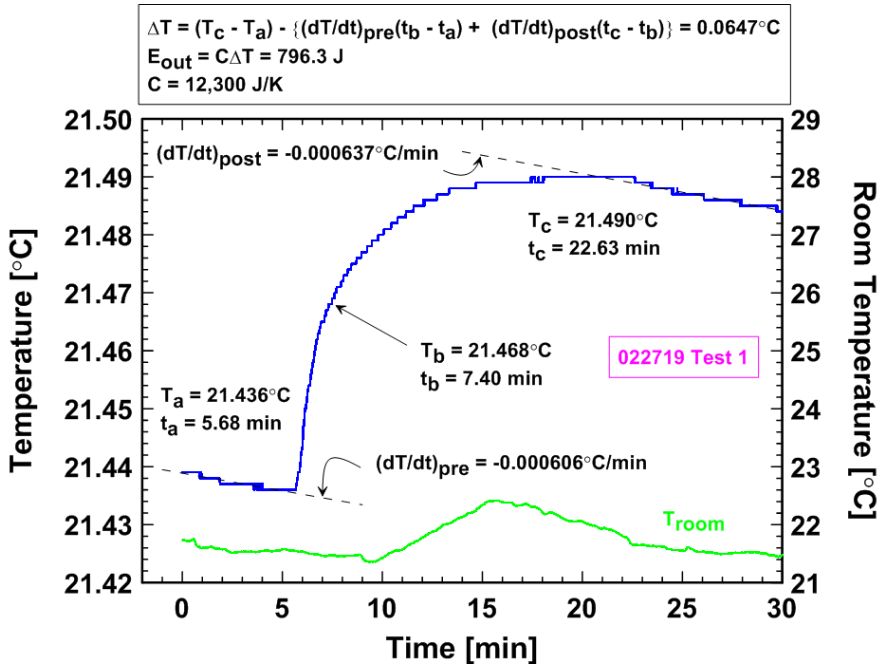

Figure A2.1. 022719 Test 1 Parr calorimetry plot

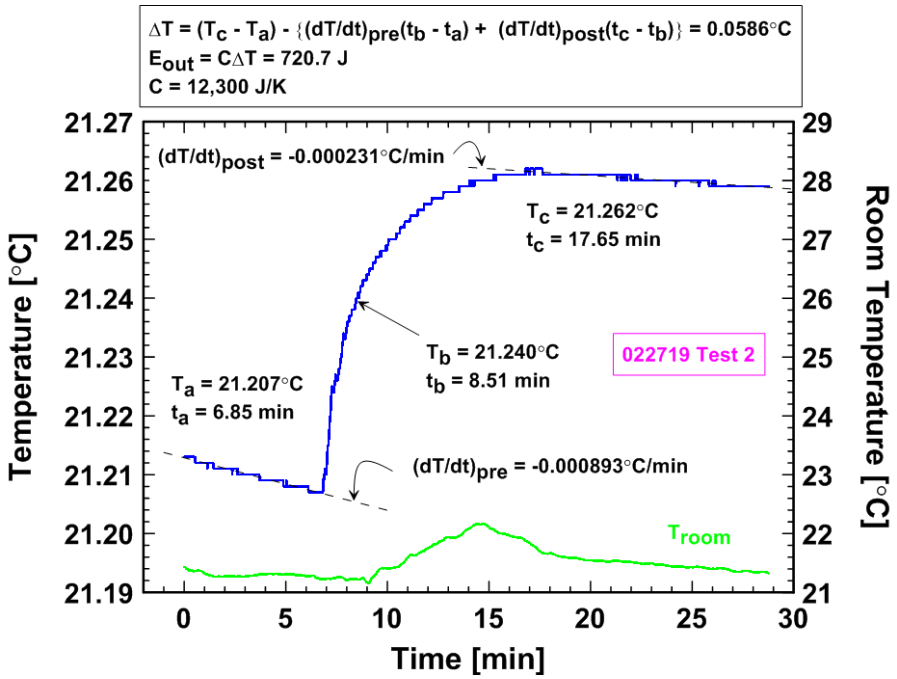

Figure A2.2. 022719 Test 2 Parr calorimetry plot

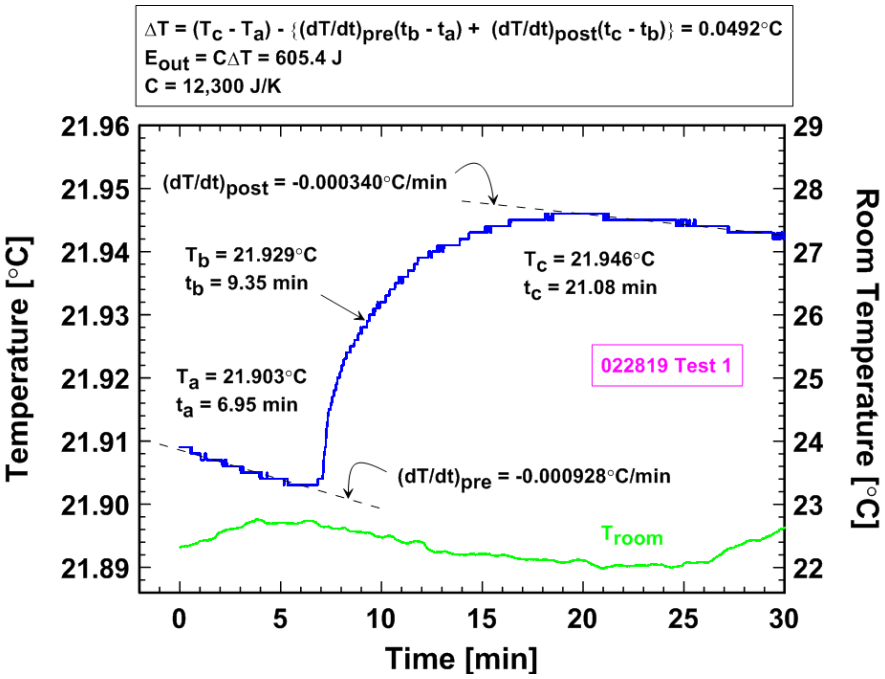

Figure A2.3. 022819 Test 1 Parr calorimetry plot

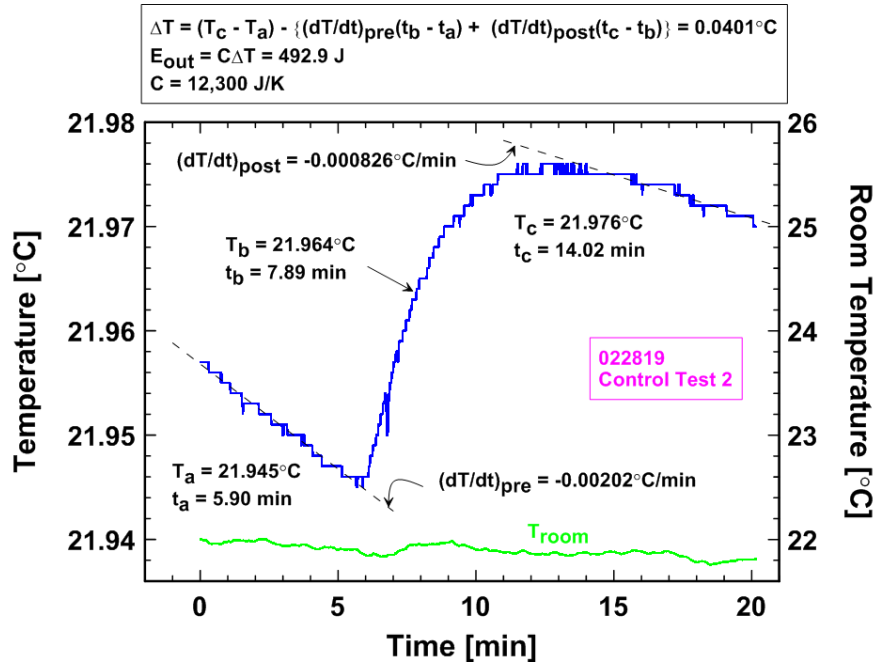

Figure A2.4. 022819 Control Test 2 Parr calorimetry plot

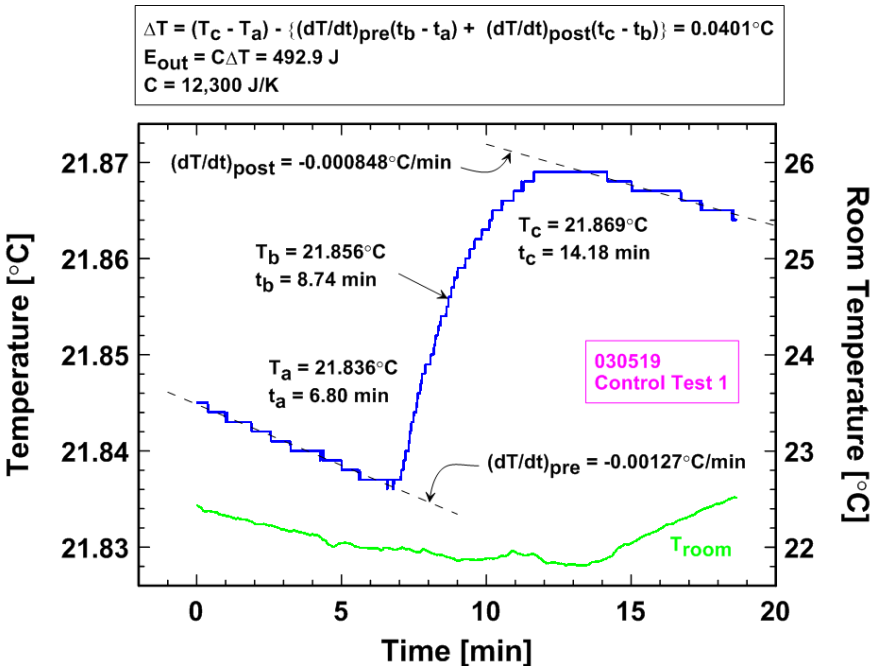

Figure A2.5. 030519 Control Test 1 Parr calorimetry plot

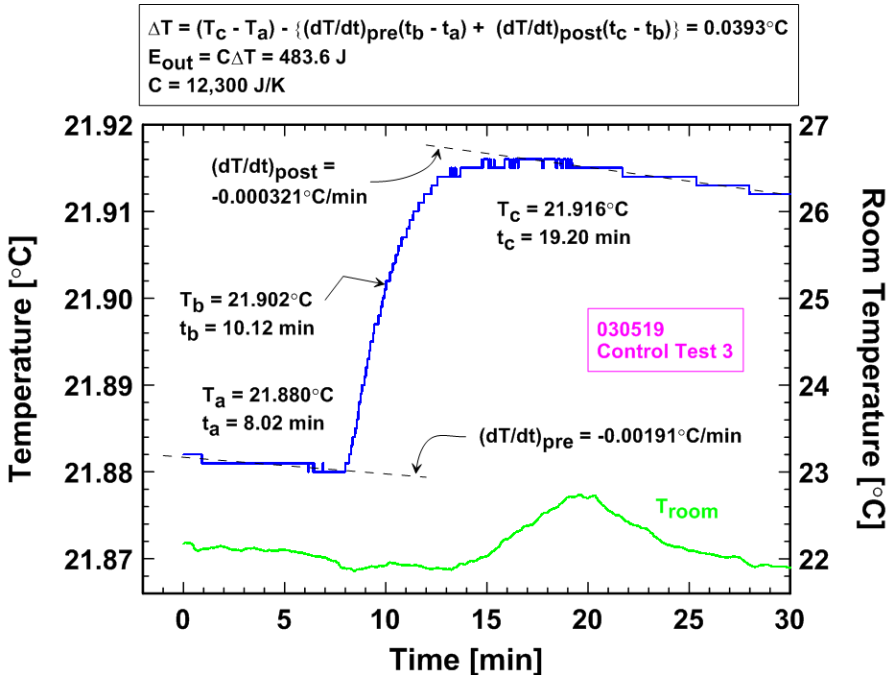

Figure A2.6. 030519 Control Test 3 Parr calorimetry plot